Peer-reviewed version available at *Crystals* **2018**, *8*, 289; doi:10.3390/cryst8070289

*Article*

# The structure of ferroselite, $FeSe_2$, at pressures up to 46 GPa and temperatures down to 50 K: A single-crystal micro-diffraction analysis

**Barbara Lavina [1], Robert T Downs [2] and Stanislav Sinogeikin [2,*]**

[1] Center for High Pressure Science & Technology Advanced Research (HPSTAR), Shanghai 201203, People's Republic of China ; barbara.lavina@icould.com

[2] Department of Geosciences, University of Arizona Tucson, Arizona 85721-0077, USA; rdowns@u.arizona.edu

[3] HPCAT, Geophysical Laboratory, Carnegie Institute of Washington, Argonne National Laboratory, Argonne, Illinois 60439, USA, ssinogeikin@carnegiescience.edu

* Correspondence: barbara.lavina@icloud.com; Tel.: +xx-xxx-xxx-xxxx

**Abstract:** We conducted an *in-situ* crystal structure analysis of ferroselite at non-ambient conditions. The aim is to provide a solid ground to further the understanding of the properties of this material in a broad range of conditions. Ferroselite, marcasite-type $FeSe_2$, was studied under high pressures up to 46 GPa and low temperatures, down to 50 K using single-crystal microdiffraction techniques. High pressure and low temperatures were generated using a diamond anvil cell and a cryostat. We found no evidences of structural instability in the explored P-T space. The deformation of the orthorhombic lattice is slightly anisotropic. As expected, the compressibility of the Se-Se dumbbell, the longer bond in the structure, is larger than that of the Fe-Se bonds. Less obvious is the behavior of the octahedral bonds, the shorter bond is the most compressible determining a small increase in the octahedron distortion with pressure. We also achieved a robust structural analysis of ferroselite at low temperature in the diamond anvil cell. Structural changes upon temperature decrease are small but qualitatively similar to those produced by pressure.

**Keywords:** $FeSe_2$; high pressure; low temperature; single crystal diffraction

Peer-reviewed version available at Crystals 2018, 8, 289; doi:10.3390/cryst8070289

## 1. Introduction

Iron selenides form economically important ore deposits and are relevant to the geochemical cycle of chalcogenides. In material science, dichalcogenides are extensively explored for solar energy applications because of their suitable thermoelectric and optical properties along with their availability and low toxicity [1], [2], [3]. Compounds with the marcasite crystal structure display a variety of intriguing physical properties intimately related to their structural arrangements[4]. Furthermore, the marcasite structure type is adopted by a number of interesting high-pressure phases such as Fe, Rh and Os pernitrides[5], [6], [7].

Ferroselite is a mineral of the chalcogenide series with end-member composition $FeSe_2$ and with the marcasite- type crystal structure. Ferroselite is the stable phase of iron diselenide at ambient conditions. Upon heating at ambient pressure $FeSe_2$ does not show phase transitions until its decomposition at 580 °C[8]; upon heating at 1200 K under moderately high pressure (65 Kbar) iron diselenide adopts the pyrite structure type [9], [10]. Iron is bonded to six selenium atoms in ferroselite, whereas selenium forms a monatomic bond and 3 bonds with iron (Fig. .1). The $FeSe_6$ edge-sharing octahedra form chains along the *c*-direction, while the Se-Se dumbbell bond lies in the *ab* plane connecting octahedral chains. In the marcasite-type structure, symmetry constrains impose some degree of distortion to the coordination geometries. The octahedron shows angular distortion and features two different bond lengths, in ferroselite those with multiplicity two are slightly shorter than the four equatorial bonds. Iron is located in 2*a* with all symmetry-constrained coordinated whereas selenium, located in 4*g*, shows variable coordinates *x* and *y*.

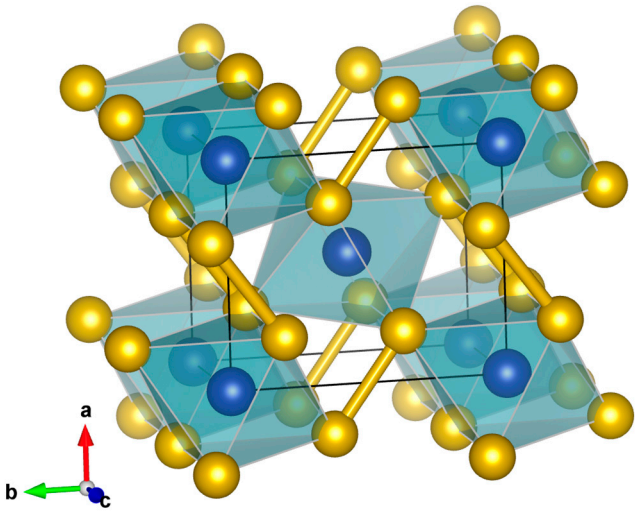


Figure .1. Representation of the crystal structure of marcasite-type $FeSe_2$ generated with VESTA[11]. Iron atoms (blue) are coordinated to 6 selenium atoms (yellow) defining a tetragonally compressed octahedron. Selenium dumbbells lie in the *ab* plane and connect the chains of octahedra running parallel to the *c*-axis.

The thermal expansion of the ferroselite lattice has been explored from ambient conditions up to decomposition temperatures[8], while magnetism and electrical

Peer-reviewed version available at Crystals 2018, 8, 289; doi:10.3390/cryst8070289

properties were explored in a broad range of temperatures [2]. Mechanically alloyed ferroselite nanocrystalline materials were studied under pressure via absorption spectroscopy up to 19 GPa, showing no evidence of phase transitions[12]. The elastic properties of $FeSe_2$ were recently determined by means of first-principles calculations [13].

In order to study the bulk and atomic response of $FeSe_2$ to external high pressure and to low temperature we performed synchrotron single-crystal microdiffraction experiments using a diamond anvil cell and a cryostat to generate target external conditions. We performed three different experiments: i) compression at ambient temperature up to ~ 46 GPa; ii) cooling down to 50 K at ambient pressure; iii) a combined high-pressure low- temperature experiment down to 110 K at 3.8 GPa. Both low-temperature experiments were conducted with single crystals loaded in a diamond anvil cell (DAC) contained in a cryostat (hereafter DAC&Cryostat).

## 2. Materials and Methods

The specimen investigated in this study is a mineral from Paradox Valley, Uravan District, Montrose County, Colorado, USA obtained from the RRUFF collection (RRUFF.info/R070461). The composition reported in the RRUFF database [14] was determined via electron micro- probe analysis. Measured elements were Se, Fe, Pb, S, Zn, Cu, Ag; within experimental resolution, the sample is pure and stoichiometric.

Conditions of high pressure and of low temperature were generated with a 4-post diamond anvil cell (DAC) and with a liquid-flow helium cryostat (Fig. .2). The DAC was equipped with conical diamonds anvils[15] of 85o aperture and 0.3 and 0.6 mm culet diameter for high pressure and low temperature data respectively. Gaskets were fabricated from pure Re or W foils; 160 and 360 μm diameter holes in the center of 35 μm thick indentations provided the sample chambers for the high-pressure and the low-temperature experiments respectively. The sample chambers were filled with pre-pressurize neon in order to maintain quasi-hydrostatic stress on the crystals in the whole range of experimental conditions.

X-ray microdiffraction data were collected at the insertion device station 16ID-B of HPCAT, Sector 16, Advanced Photon Source, Argonne National Laboratory. Experiments were performed using hard x-rays (λ=0.40662, 0.36793 Å) focused to about 5x5 μm FWHM at the sample position. The experimental station was equipped with a heavy-duty motorized sample stage suitable for measurements with a cryostat for high pressure studies. The cryostat provided wide angular x-ray access and was equipped with a gas membrane for pressure control. Diffracted X-rays were collected with the rotation method using a MAR165-CCD area detector and a MAR345IP detector, which was calibrated using powder patterns of $CeO_2$ standard and the GSASII software [16]. The rotation range was 72o for high-pressure data and 60o for low- temperature data, the x-ray access was reduced by

the gas membrane and cryostat body in the latter case. For the samples in the cryostat diffraction images were collected with the detector (CCD) at three different locations in the horizontal direction perpendicular to the beam. The maximum resolution achieved was 0.6 Å.

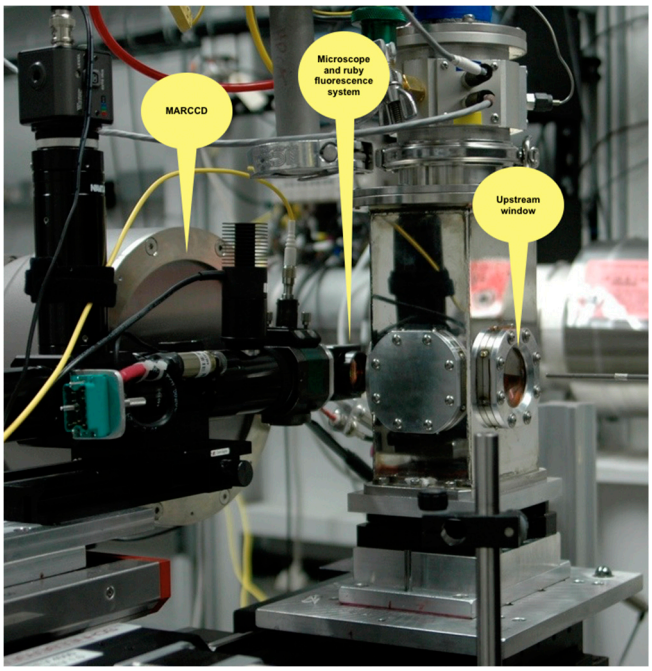


Figure .2. Cryostat for combined high-pressure and low-temperature conditions mounted on the sample stage of the 16ID-B beamline of the APS, ANL.

Pressure was calibrated using the equation of state of platinum[17] for ambient temperature data and ruby[18] for low-temperature data. Temperature was measured us- ing silicon diode thermocouples positioned on the DAC body and on the copper block, the two differ by less than two degrees during data collection. Data reduction was performed GSE_ADA & RSV[19] , WinGX[20], and DIOPTAS[21]. Structural refinements were carried out using Shelxl [22]. Standard powder patterns were analyzed with GSASII[16].

## 3. Results and discussion

### *3.1Ambient conditions structural refinements*

Measuring structure factors in the diamond anvil cell with micron-sized x-ay beams is an established technique providing extremely valuable and robust results in spite of its challenges. In addition to high-pressure measurements, here we collected data from small single crystals loaded in the DAC which was then loaded in a cryostat (Fig. .2). The cryostat we used for high pressure measurements is a relatively bulky device with several connections, the most cumbersome being the liquid helium supply line and the vacuum line. These connections pull the sample stage causing an increase in the sphere of confusion of the rotation axis. Because crystals are roughly 20 μm in diameter and the beam is around 5 μm FWHM, we

Preprints (www.preprints.org) | NOT PEER-REVIEWED | Posted: 12 June 2018 doi:10.20944/preprints201806.0183.v1

Peer-reviewed version available at Crystals 2018, 8, 289; doi:10.3390/cryst8070289

anticipated that the x-ray flux on the crystals would vary more dramatically during data collection compared with ambient temperature measurements. As a consequence, the set of observed structure factors would not be in scale. Furthermore, for relatively low-symmetry crystals, a reliable empirical correction calculated from comparing sets of equivalent reflections might be difficult to define due to the low data redundancy. In order to compensate for such effects we loaded three crystals with different crystallographic orientations in the diamond anvil cell for low temperature work. Furthermore, we collected several rotation images in a small grid fashion around the crystal center for a few datapoint. In table I literature data are compared with some of our results. All data collections were performed with samples in environmental cells, DAC and DAC&cryostat, before conditions were changed. In addition to the scale factor, we refined the two symmetry- unconstrained fractional coordinates of Se and isotropic displacement parameters for both atoms for a total of 5 variables. Overall results are in good agreement. We note that: i) because we always measured a good number of reflections and we only had 2 positional parameters to refine for the heavier element, these were always reason- able, including high R factors refinements; ii) merging grid diffraction patterns provided in most cases excellent results and low disagreements between equivalent reflections and better results than empirical corrections; iii) datasets are not uniform because, we infer, the increase in the sphere of confusion caused by the cryostat is not fully reproducible. In conclusion, it appears beneficial to acquire redundant datasets, this allow adopting different data reduction strategies and provide the best likelihood that robust refinements can be obtained.

**Table 1.** AMBIENT-CONDITIONS UNIT-CELL PARAMETERS AND ATOMIC FRACTIONAL

| | $N_{all}$, $N_{ind}$ | $a$ (Å) | $b$ (Å) | $c$ (Å) | $R_{eq}$, $R_1$(%) | $x$ (Se) | $y$ (Se) | $U_{eq}$-Fe (Å$^2$) | $U_{eq}$-Se (Å$^2$) |
|---|---|---|---|---|---|---|---|---|---|
| Ref.[23] | | 4.8002(4) | 5.7823(5) | 3.5834(4) | | 0.2127(6) | 0.3701(5) | | |
| Ref.[24] | | 4.804(2) | 5.784(3) | 3.586(2) | | 0.2134(2) | 0.3690(1) | | |
| RRUFF.info/R070461[a)] | | 4.795(3) | 5.777(4) | 3.584(1) | | - | - | | |
| Ref. [2] | | 4.8031(6) | 5.7849(2) | 3.5840(4) | | 0.2127(2) | 0.3691(7) | | |
| DAC | 204, 98, | 4.801(3) | 5.787(2) | 3.5859(7) | 12, 4.9 | 0.2135(3) | 0.3692(1) | 0.0095(5) | 0.0099(5) |
| DAC & cryostat C1[b)] | 205, 82 | 4.804(4) | 5.781(3) | 3.5814(7) | 8.4, 4.4 | 0.2133(3) | 0.3692(1) | 0.0056(5) | 0.0059(4) |
| DAC&Cryostat C2[c)] | 253,103, | 4.8016(9) | 5.7772(15) | 3.5850(8) | 9.6, 5.4 | 0.2137(2) | 0.36921(13) | 0.0090(5) | 0.0090(4) |
| DAC& cryostat C3[b)] | 214, 94 | 4.7993(14) | 5.785(2) | 3.5820(4) | 33, 12 | 0.2130(7) | 0.3699(3) | 0.0067(12) | 0.0086(10) |

COORDINATES FROM THE LITERATURE AND FROM THIS WORK (SEE TEXT).

[a)]same specimen of the present work; [b)] no grid scan, no empirical corrections; [c)]three detector positions, *hkl* from merged grid scans, no empirical corrections

## *3.2 High pressure*

Diffraction data of ferroselite were collected up to 46 GPa. There are no indications of phase transitions but the highest pressure pattern shows moderate peak

broadening that might be the result of non hydrostatic stress as well as the manifestation of an incipient phase transition. The datapoint at 3.63 GPa was collected with the DAC&cryostat before decreasing temperature, structural parameters at this pressure are in the same trend of data collected in the DAC, confirming our ability to collect full datasets in these conditions without introducing systematic errors in our analysis. The anisotropy of the deformation of the orthorhombic cell of ferroselite under quasi-hydrostatic compression is clear after 17 GPa. As shown in Fig. .3 the lattice is more compressible in the direction of the *a*-axis and is stiffer along the *b*-axis. This observation is consistent with the recently predicted behavior[13]. The bulk compression of marcasite-$FeSe_2$ can be modeled by a second-order Birch−Murnaghan EoS with an ambient bulk modulus of 121.6 GPa. Although we collected too few datasets to reliably fit a third order EoS, it can be inferred from the plot in Fig. .4 that a third order EoS might be more appropriate to describe the compressibility of this material, and indeed values significantly larger than 4 for $K_0$' have been suggested for $FeS_2$ marcasite[25] and several other marcasite-type chalcogenides. Fixing $K_0$' to 4.6, a value that both leads to best fitting and is close to the value in marcasite, and using the third- order Birch−Murnaghan EoS results in a $K_0$ of 114.1 GPa. We could not however satisfactorily fit our data with the same EoS equation and using the recently proposed bulk modulus 74.7 GPa[13].

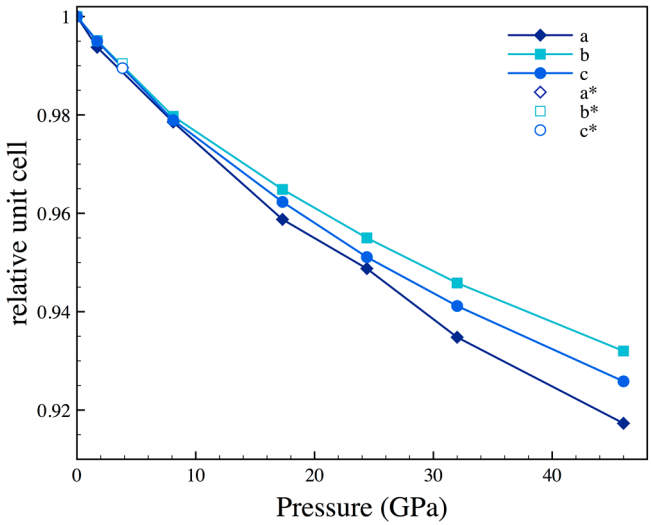


Figure .3. Relative compression of the orthorhombic unit-cell edges.

Robust crystal structure analysis allow exploring the changes in atomic arrangement with pressure. Fig. .5 shows the pressure dependence of interatomic distances and their relative changes. As could be expected, the longest bond, the Se-Se dumbbell, shows the greatest compressibility. The octahedral bonds however show a less obvious behavior, with the shorter bond being more compressible than the longer bond, hence the octahedral distortion increases with pressure.

Peer-reviewed version available at Crystals 2018, 8, 289; doi:10.3390/cryst8070289

**Table 2.** UNIT CELL PARAMETERS AND ATOMIC FRACTIONAL COORDINATES OF FERROSELITE AT HIGH PRESSURE.

| P (GPa) | a (Å) | b (Å) | c (Å) | x (Se) | y (Se) | $U_{eq}$-Fe (Å$^2$) | $U_{eq}$-Se (Å$^2$) |
|---|---|---|---|---|---|---|---|
| 1.7 | 4.771(2) | 5.756(1) | 3.5663(6) | 0.2129(4) | 0.36884(13) | 0.0079(6) | 0.0083(5) |
| 3.83* | 4.751(2) | 5.729(2) | 3.5467(11) | 0.2125(6) | 0.3687(7) | 0.014(2) | 0.013(2) |
| 8.1 | 4.698(3) | 5.667(2) | 3.5088(7) | 0.2123(6) | 0.3688(2) | 0.0083(8) | 0.0090(7) |
| 17.3 | 4.603(3) | 5.581(2) | 3.4492(9) | 0.2123(3) | 0.36854(9) | 0.0085(5) | 0.0088(5) |
| 24.4 | 4.555(2) | 5.524(12) | 3.4090(5) | 0.2114(4) | 0.3683(2) | 0.0066(9) | 0.0057(7) |
| 32 | 4.488(4) | 5.471(3) | 3.3734(11) | 0.2111(6) | 0.3676(2) | 0.0063(13) | 0.0064(12) |
| 46 | 4.404(3) | 5.391(2) | 3.3185(9) | 0.2103(4) | 0.36689(13) | 0.0066(9) | 0.0070(8) |

* DAC&cryostat measurement, refinement from merged grid scan images

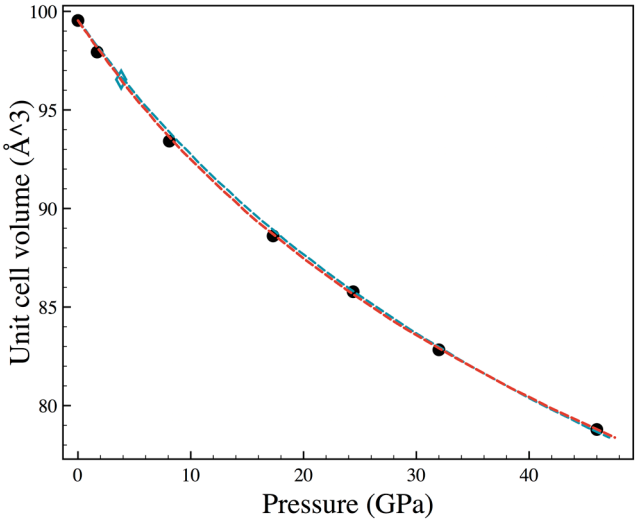


Figure .4. Bulk compressibility of $FeSe_2$. The blue symbol shows data collected at ambient pressure in DAC&cryostat. The black line shows a second order Birch−Murnaghan EoS fit, the red line a third order Birch−Murnaghan EoS fit (see text).

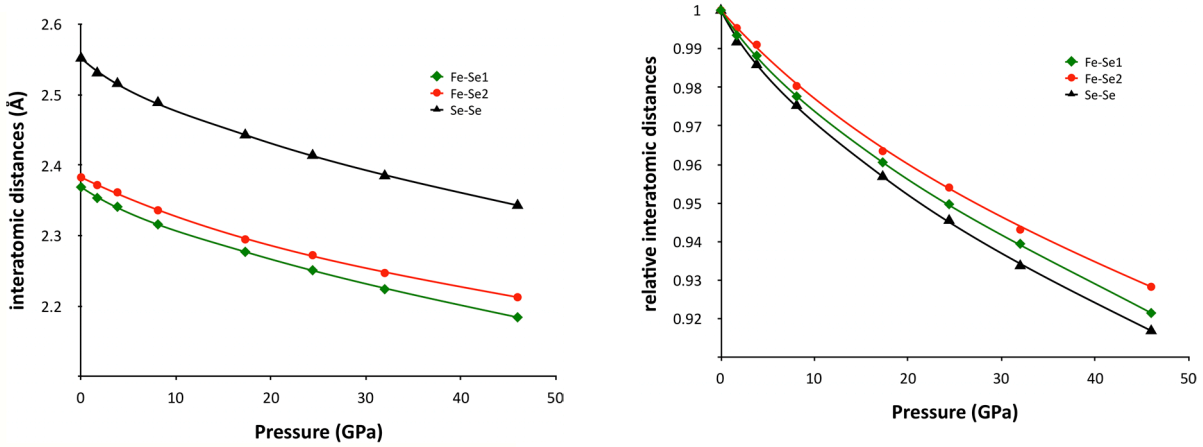


(a) (b)

Figure .5. Absolute (a) and relative (b) interatomic distances as a function of pressure. Uncertainties are smaller than the symbols' sizes.

### *3.3 Low Temperature*

Structural data of $FeSe_2$ were collected ambient pressure at three temperatures 198.2, 148.4, and 50.4 K and at about 3.7 GPa at 197 and 116 K (Table. III). Upon attempting to maintain a constant pressure in the sample chamber during further cooling by increasing the gas membrane pressure, the experiment failed abruptly when the load on the DAC applied with the gas membrane was rapidly transferred to the diamond anvils upon overcoming the DAC friction.

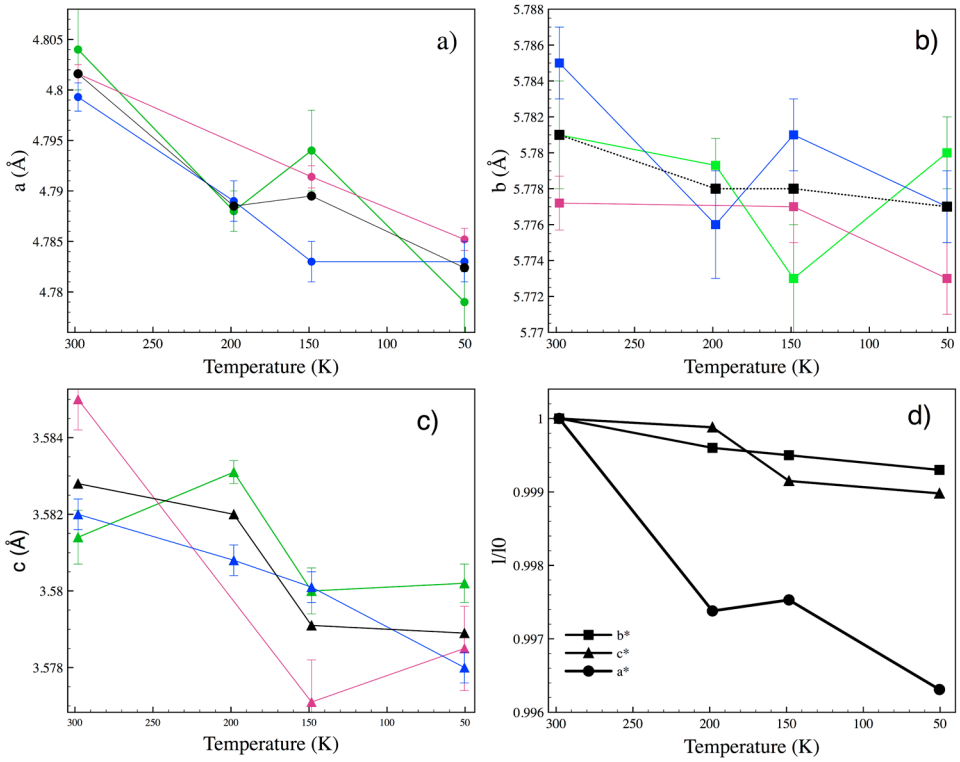


Figure .6. Absolute and relative variation of the unit cell parameters lengths as a function of temperature at ambient pressure. Red, Blue and green symbols: different crystals in the same sample chamber; black: weighted average of the three crystals.

We expected the effect on structural parameters of lowering temperature from 300 to 50 K to be small, close to the resolution of our experiment. Hence we loaded three crystals with different orientations for this experiment in order to obtain a more complete sampling of the reciprocal space and increase data redundancy. Because of the limited access to the reciprocal space different crystallographic directions can be probed with different precision in differ- ently oriented crystals as can be seen inspecting error bars in Fig. .6A-C. Plots of unit cell variations of individual crystals hardly show discernible trends, however trends are appreciable when weighted average are considered (Fig. .6, black symbols). As for the high pressure behavior and for the high temperature behavior[8] , the greatest lattice parameters variations are observed in the direction of the *a*-axis (Fig. .6D) . Unit-cell edges variations along the other principal axes are close to uncertainties. Variations of the Fe-Se bond lengths are also within uncertainties as shown in Fig. .8, the Se-Se bond decreases from 2.552 Å to 2.537 Å.

The anisotropy of the lattice at low temperature is qualitatively similar to that observed at high pressure. The unit cell volume decreases by ~0.6 % upon cooling from ambient temperatures down to 50 K, a change that corresponds to a pressure of 0.8-0.9 GPa depending on the EoS adopted (see above).

We were able to collected just two pressure points at combined low temperature and high pressure (Table III). Variations on the structure of ferroselite induced by temperature at this pressure are within uncertainties.

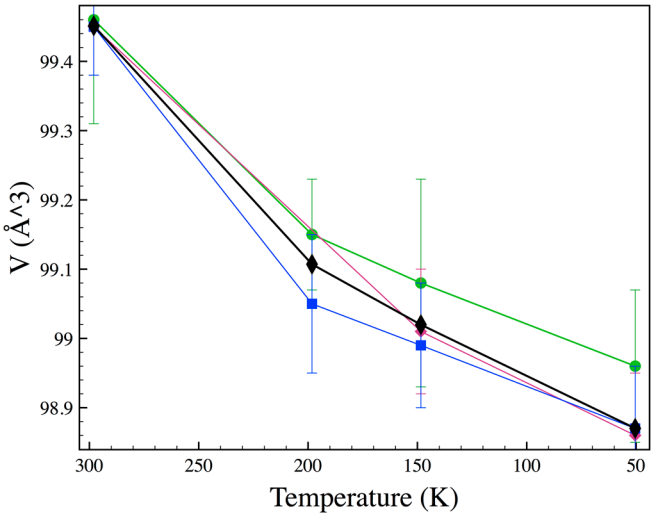


Figure .7. Variation of the unit cell volume as a function of temperature at ambient pressure.

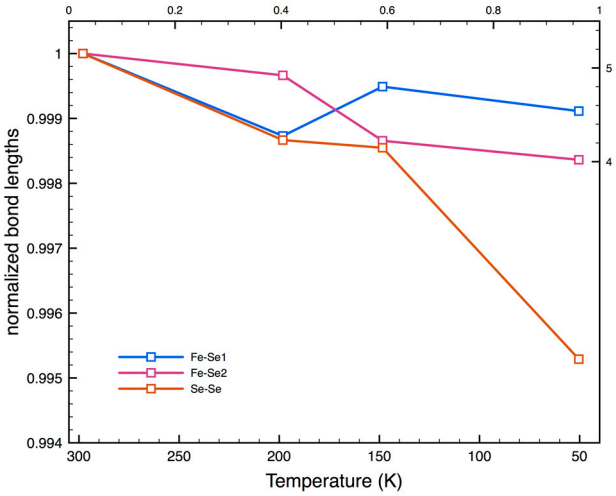


Figure .8. Normalized bond lengths vs temperature at ambient pressure.

**Table 3.** UNIT CELL PARAMETERS AND ATOMIC FRACTIONAL COORDINATES AT LOW TEMPERATURE AND BOTH AMBIENT PRESSURE AND HIGH PRESSURE. FOR AMBIENT PRESSURE, WEIGHED AVERAGES OF THREE CRYSTALS ARE REPORTED.

| T (K) | P (GPa) | a (Å) | b (Å) | c (Å) | x (Se) | y (Se) |
|---|---|---|---|---|---|---|
| 198.2 | $10^{-4}$ | 4.7885 | 5.7782 | 3.5821 | 0.2148(4) | 0.3692(2) |
| 148.4 | $10^{-4}$ | 4.7893 | 5.7775 | 3.5795 | 0.2135(2) | 0.3691(2) |
| 50.4 | $10^{-4}$ | 4.7834 | 5.7767 | 3.5789 | 0.2138(3) | 0.3694(2) |
| 197 | 3.68 | 4.7512) | 5.723(2) | 3.5501(11) | 0.2131(7) | 0.3699(6) |
| 116 | 3.64 | 4.7446(11) | 5.772(2) | 3.5512(8) | 0.2130(6) | 0.3695(7) |

## 5. Conclusions

The physical properties of materials important for critical technologies such as solar energy ought to be defined in great detail. Studying a material's behavior in a broad range of conditions allows more stringent constraints to modeling hence a better general understanding of the material. We conducted a detailed examination of the crystal structure of marcasite-type iron diselenide at pressures up to 46 GPa, temperatures down to 50.4 K and combined high pressure and low temperature conditions of ~ 3.8 GPa and 197 and 116 K. The phase shows no clear signs of phase transitions in this range, even though it is probably metastable at the highest pressures, considering that it transforms to the pyrite structure above ~ 6.5 GPa upon heating[9]. We described in details the anisotropy of the lattice response to external conditions and changes in the atomic arrangement.

Maintaining sufficient centering of microcrystals while performing rotation data collections of samples in bulky environmental cells such as combined DAC and cryostat is challenging and not necessarily reproducible. Hence we find that collecting redundant datasets, in this case grid scans, is the safest way to gather datasets from which reliable structure factors can be extracted. Multiple crystal orientations allow obtaining a uniform precision in lattice parameters determinations in addition to better coverage of the reciprocal space.

**Author Contributions:** For research articles with several authors, a short paragraph specifying their individual contributions must be provided. The following statements should be used "Conceptualization, B.L.; Methodology, B.L.; Formal Analysis, B.L.; Investigation, B.L.; Resources, B.L., R.T.D and S.S.; Writing-Original Draft Preparation, B.L.; Writing-Review & Editing, B.L.; Visualization, B.L.; Project Administration, B.L.; Funding Acquisition, B.L.".

**Funding:** This research was sponsored by the DOE-NNSA under Cooperative Agreement No. DE-FC52-06NA262740. This work was conducted at HPCAT (Sector 16), Advanced Photon Source (APS), Argonne National Laboratory. HPCAT operations are supported by DOE-NNSA under Award No. DE-NA0001974, with partial instrumentation funding by NSF. The Advanced Photon Source is a U.S. Department of Energy (DOE) Office of Science User Facility operated for the DOE Office of Science by Argonne National Laboratory under Contract No. DE-AC02-06CH11357. Use of the COMPRES-GSECARS gas loading system was supported by COMPRES under NSF Cooperative Agreement EAR 11- 57758 and by GSECARS through NSF Grant EAR-1128799 and DOE Grant DE-FG02- 94ER14466.

**Conflicts of Interest:** "The authors declare no conflict of interest."

## References

[1] Kanchana, V., Vaitheeswaran, G., Valsakumar, C., M. & Mahanti, S. D. Thermoelectric properties of marcasite and pyrite $FeX_2$ (X = Se, Te): a first principle study. *RSC Advances* 4, 9424–9431 (2014).

[2] Li, G. *et al.* Effect of vacancies on magnetism, electrical transport, and thermoelectric performance of marcasite $FeSe_{2-d}$ (d=0.05). *Chemistry of Materials* 27, 8220–8229 (2015).

[3] Ghosh, A. & Thangavel, R. Electronic structure and optical properties of iron based chalcogenide $FeX_2$ (X = S, Se, Te) for photovoltaic applications: a first principle study. *Indian Journal of Physics* 91, 1339–1344 (2017).

[4] Goodenough, J. B. Energy bands in $TX_2$ compounds with pyrite, marcasite, and arsenopyrite structures. *Journal of Solid State Chemistry* 5, 144 – 152 (1972).

[5] Wang, Y. X. & Arai, T., Masao ans Sasaki. Marcasite osmium ni- tride with high bulk modulus: First-principles calculations. *Applied Physics Letters* 90, 061922 (2007).

[6] Niwa, K. *et al.* High pressure synthesis of marcasite-type rhodium pernitride. *Inorganic Chemistry* 53, 697–699 (2014).

[7] Wang, Z. *et al.* Prediction and characterization of the marcasite phase of iron pernitride under high pressure. *Journal of Alloys and Compounds* 702, 132 – 137 (2017).

[8] Kjekshus, A. & Rakke, T. Compounds with the marcasite type crystal structure. XI. High temperature studies of chalcogenides. *Acta Chemica Scandinavica* A29, 443–452 (1975).

[9] Bither, T. *et al.* New transition metal dichalcogenides formed at high pressure. *Solid State Communications* 4, 533 – 535 (1966).

[10] Bither, T. A., Bouchard, R. J., Cloud, W. H., Donohue, P. C. & Siemons, W. J. Transition metal pyrite dichalcogenides. high- pressure synthesis and correlation of properties. *Inorganic Chem- istry* 7, 2208–2220 (1968).

[11] Momma, K. & Izumi, F. *VESTA3* for three-dimensional visualiza- tion of crystal, volumetric and morphology data. *Journal of Applied Crystallography* 44, 1272–1276 (2011).

[12] Campos, C. E. M. *et al.* Pressure-induced effects on the struc- tural properties of iron selenides produced by mechano-synthesis. *Journal of Physics: Condensed Matter* 16, 8485 (2004).

[13] Tian, X.-H. & Zhang, J.-M. The structural, elastic, electronic and optical properties of orthorhombic $FeX_2$ (X=S, Se, Te). *Superlat- tices and Microstructures* 119, 201 – 211 (2018).

[14] Lafuente, B., Downs, R. T., Yang, H. & Stone, N. The power of databases: the RRUFF project. In: Highlights in Mineralogical Crystallography, T Armbruster and R M Danisi, eds. Berlin, Germany, W. De Gruyter 1–30 (2015).

[15] Boehler, R. & De Hantsetters, K. New anvil designs in diamond- cells. *High Pressure Research* 24, 391–396 (2004).

[16] Toby, B. H. & Von Dreele, R. B. *GSAS-II*: the genesis of a modern open-source all purpose crystallography software package. *Journal of Applied Crystallography* 46, 544–549 (2013).

[17] Matsui, M. *et al.* The temperature-pressure-volume equation of state of platinum. *Journal of Applied Physics* 105 (2009).

[18] Mao, H., Xu, J. & Bell, P. Calibration of the ruby pressure gauge to 800-Kbar under quasi-hydrostatic conditions. *Journal of Geophysical Research-Solid Earth and Planets* 91, 4673–4676 (1986).

[19] Dera, P. *et al.* High pressure single-crystal micro x-ray diffraction analysis with gse ada andrsv software. *High Pressure Research* 33, 466–484 (2013).

[20] Farrugia, L. J. WinGX and ORTEP for Windows: an update. Journal of Applied Crystallography 45, 849–854 (2012).

[21] Prescher, C. & Prakapenka, V. B. DIOPTAS: a program for reduc- tion of two-dimensional X-ray diffraction data and data exploration. *High Pressure Research* 35, 223–230 (2015).

[22] Sheldrick, G. M. A short history of SHELX. *Acta Crystallograph- ica Section a* 64, 112–122 (2008).

[23] Kjekshus, A., Rakke, T. & Andresen, A. F. Compounds with the marcasite type crystal structure. IX. Structural data for $FeAs_2$, $FeSe_2$, $NiAs_2$, $NiSb_2$ and $CuSe_2$. *Acta Chemica Scandinavica A* 28, 996–1000 (1974).

[24] Pickardt, J., Reuter, B., Riedel, E. & Söchtig, J. On the formation of $FeSe_2$ single crystals by chemical transport reactions. *Journal of Solid State Chemistry* 15, 366 – 368 (1975).

[25] Tian, X.-H. & Zhang, J.-M. The structural, elastic and electronic properties of marcasite fes2 under t pressure. *Journal of Physics and Chemistry of Solids* 118, 88–94 (2018).